Acoustophoresis in Wet-Etched Glass Chips

ARTICLE *in* ANALYTICAL CHEMISTRY · AUGUST 2008

Impact Factor: 5.64 · DOI: 10.1021/ac800572n · Source: PubMed

4 AUTHORS, INCLUDING:

Mikael Evander
Lund University
27 PUBLICATIONS **594** CITATIONS
SEE PROFILE

Andreas Lenshof
Lund University
24 PUBLICATIONS **1,385** CITATIONS
SEE PROFILE

Johan Nilsson
Lund University
98 PUBLICATIONS **2,418** CITATIONS
SEE PROFILE

Anal. Chem. **2008,** *80,* 5178–5185

Acoustophoresis in Wet-Etched Glass Chips

Mikael Evander,* Andreas Lenshof, Thomas Laurell, and Johan Nilsson

The Department of Electrical Measurements, Lund University, P.O. Box 118, 211 00 Lund, Sweden

Acoustophoresis in microfluidic structures has primarily been reported in silicon microfabricated devices. This paper demonstrates, for the first time, acoustophoresis performed in isotropically etched glass chips providing a performance that matches that of the corresponding silicon microdevices. The resonance mode characteristics of the glass chip were equal to those of the silicon chip at its fundamental resonance. At higher order resonance modes the glass chip displays resonances at lower frequencies than the silicon chip. The cross-sectional profiles of acoustically focused particle streams are also reported for the first time, displaying particles confined in a vertical band in the channel center for both glass and silicon chips. A particle extraction efficiency of 98% at flow rates up to 200 μL/min (2% particle concentration) is reported for the glass chip at the fundamental resonance. The glass and silicon chips displayed equal particle extraction performance when tested for increasing particle concentrations of 2−15%, at a flow velocity of 12.9 cm/s for the glass chip and 14.8 cm/s for the silicon chip.

Continuous separation of cells and particles by means of microsystem technology and microfluidics is gaining increased interest in the biomedical and biochemical field. Several techniques are available that either use externally induced forces as the separation mechanism or the geometry of the microfluidic device itself as the separating element. Magnetophoresis[1–3] and dielectrophoresis[4–6] are using magnetic and electric fields, respectively, whereas pinched flow fractionation,[7–9] hydrodynamic filtration,[10–12] and obstacle induced separation[13–15] rely on the combination of laminar flow and the channel geometry. Another alternative for separation with externally induced forces is the use of acoustic forces, acoustophoresis, which is the topic of this paper.

Acoustic forces in microsystems have proven to be a very versatile and gentle tool for on-chip handling of particles and cells. The forces created by standing waves can be used for such diverse tasks as eliminating lipid emboli from shed blood in thoracic surgery,[16,17] blood component fractionation and particle sizing,[18] contaminated blood plasma replacement[19] and buffer media exchange,[20] specific selection of affinity binding phages from bacteriophage libraries,[21] rare event selection,[22] positioning,[23–25] and trapping.[26–28] In addition, several investigations in both macrosystems[29,30] and microsystems[17,26,31,32] have shown that no adverse effects related to the acoustic handling can be seen on cells.

Commonly, the standing wave is formed between two parallel walls, using one wall as an ultrasonic transmitter and the other wall as a reflector. Rectangular geometries with vertical walls have most commonly been used, but systems using focused sound waves have also been reported.[33] The standing wave can be formed either between the bottom and the top of a fluidic channel,

* To whom correspondence should be addressed. Phone: +46-46-222 75 27. Fax: +46-46-222 45 27. E-mail: Mikael.Evander@elmat.lth.se.

(1) Pamme, N.; Manz, A. *Anal. Chem.* **2004**, *76*, 7250–7256.
(2) Pamme, N. *Lab Chip* **2006**, *6*, 24–38.
(3) Han, K. H.; Frazier, A. B. *Lab Chip* **2006**, *6*, 265–273.
(4) Gonzalez, C. F.; Remcho, V. T. *J. Chromatogr., A* **2005**, *1079*, 59–68.
(5) Doh, I.; Cho, Y. H. *Sens. Actuators, A* **2005**, *121*, 59–65.
(6) Hu, X. Y.; Bessette, P. H.; Qian, J. R.; Meinhart, C. D.; Daugherty, P. S.; Soh, H. T. *Proc. Natl. Acad. Sci. U.S.A.* **2005**, *102*, 15757–15761.
(7) Yamada, M.; Nakashima, M.; Seki, M. *Anal. Chem.* **2004**, *76*, 5465–5471.
(8) Takagi, J.; Yamada, M.; Yasuda, M.; Seki, M. *Lab Chip* **2005**, *5*, 778–784.
(9) Zhang, X. L.; Cooper, J. M.; Monaghan, P. B.; Haswell, S. J. *Lab Chip* **2006**, *6*, 561–566.
(10) Yamada, M.; Seki, M. *Lab Chip* **2005**, *5*, 1233–1239.
(11) Yamada, M.; Seki, M. *Anal. Chem.* **2006**, *78*, 1357–1362.
(12) Yang, S.; Undar, A.; Zahn, J. D. *Lab Chip* **2006**, *6*, 871–880.
(13) Huang, L. R.; Cox, E. C.; Austin, R. H.; Sturm, J. C. *Science* **2004**, *304*, 987–990.
(14) Davis, J. A.; Inglis, D. W.; Morton, K. J.; Lawrence, D. A.; Huang, L. R.; Chou, S. Y.; Sturm, J. C.; Austin, R. H. *Proc. Natl. Acad. Sci. U.S.A.* **2006**, *103*, 14779–14784.
(15) Inglis, D. W.; Davis, J. A.; Austin, R. H.; Sturm, J. C. *Lab Chip* **2006**, *6*, 655–658.
(16) Petersson, F.; Nilsson, A.; Holm, C.; Jonsson, H.; Laurell, T. *Analyst* **2004**, *129*, 938–943.
(17) Jönsson, H.; Holm, C.; Nilsson, A.; Petersson, F.; Johnsson, P.; Laurell, T. *Ann. Thorac. Surg.* **2004**, *78*, 1572–1578.
(18) Petersson, F.; Aberg, L.; Sward-Nilsson, A. M.; Laurell, T. *Anal. Chem.* **2007**, *79*, 5117–5123.
(19) Petersson, F.; Nilsson, A.; Jonsson, H.; Laurell, T. *Anal. Chem.* **2005**, *77*, 1216–1221.
(20) Hawkes, J. J.; Barber, R. W.; Emerson, D. R.; Coakley, W. T. *Lab Chip* **2004**, *4*, 446–452.
(21) Augustsson, P.; Persson, J.; Ohlin, M.; Laurell, T. *Proceedings of Micro Total Analysis Systems*, Paris, France, 2007; pp 1813−1815.
(22) Grenvall, C.; Augustsson, P.; Petersson, F.; Laurell, T. *Proceedings of Micro Total Analysis Systems*, Paris, France, 2007; pp 1813−1815.
(23) Neild, A.; Oberti, S.; Beyeler, F.; Dual, J.; Nelson, B. J. *J. Micromech. Microeng.* **2006**, *16*, 1562–1570.
(24) Neild, A.; Oberti, S.; Radziwill, G.; Dual, J. *Biotechnol. Bioeng.* **2007**, *97*, 1335–1339.
(25) Hawkes, J. J.; Long, M. J.; Coakley, W. T.; McDonnell, M. B. *Biosens. Bioelectron.* **2004**, *19*, 1021–1028.
(26) Evander, M.; Johansson, L.; Lilliehorn, T.; Piskur, J.; Lindvall, M.; Johansson, S.; Almqvist, M.; Laurell, T.; Nilsson, J. *Anal. Chem.* **2007**, *79*, 2984–2991.
(27) Spengler, J. F.; Coakley, W. T. *Langmuir* **2003**, *19*, 3635–3642.
(28) Svennebring, J.; Manneberg, O.; Wiklund, M. *J. Micromech. Microeng.* **2007**, 2469.
(29) Pui, P. W. S.; Trampler, F.; Sonderhoff, S. A.; Gröschl, M.; Kilburn, D. G.; Piret, J. M. *Biotechnol. Prog.* **1995**, *11*, 146–152.
(30) Doblhoffdier, O.; Gaida, T.; Katinger, H.; Burger, W.; Groschl, M.; Benes, E. *Biotechnol. Prog.* **1994**, *10*, 428–432.
(31) Hultström, J.; Manneberg, O.; Dopf, K.; Hertz, H. M.; Brismar, H.; Wiklund, M. *Ultrasound Med. Biol.* **2007**, *33*, 145–151.
(32) Bazou, D.; Kuznetsova, L. A.; Coakley, W. T. *Ultrasound Med. Biol.* **2005**, *31*, 423–430.
(33) Wiklund, M.; Toivonen, J.; Tirri, M.; Hanninen, P.; Hertz, H. M. *J. Appl. Phys.* **2004**, *96*, 1242–1248.

10.1021/ac800572n CCC: $40.75
Published on Web 05/20/2008

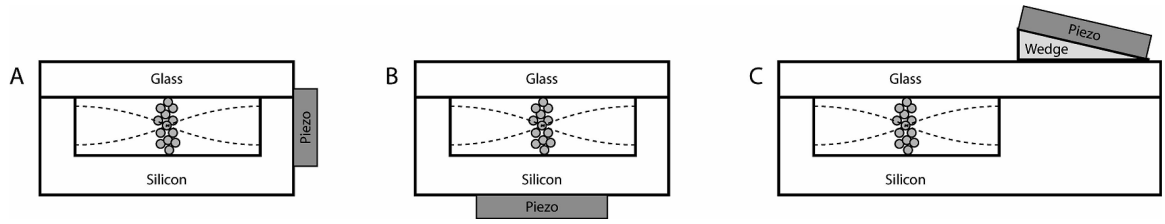

Figure 1. (A) The acoustic standing wave is induced parallel to the wave propagation. (B) The standing wave is induced perpendicular to the primary wave propagation. (C) A wedge is used to couple the waves into the cavity.

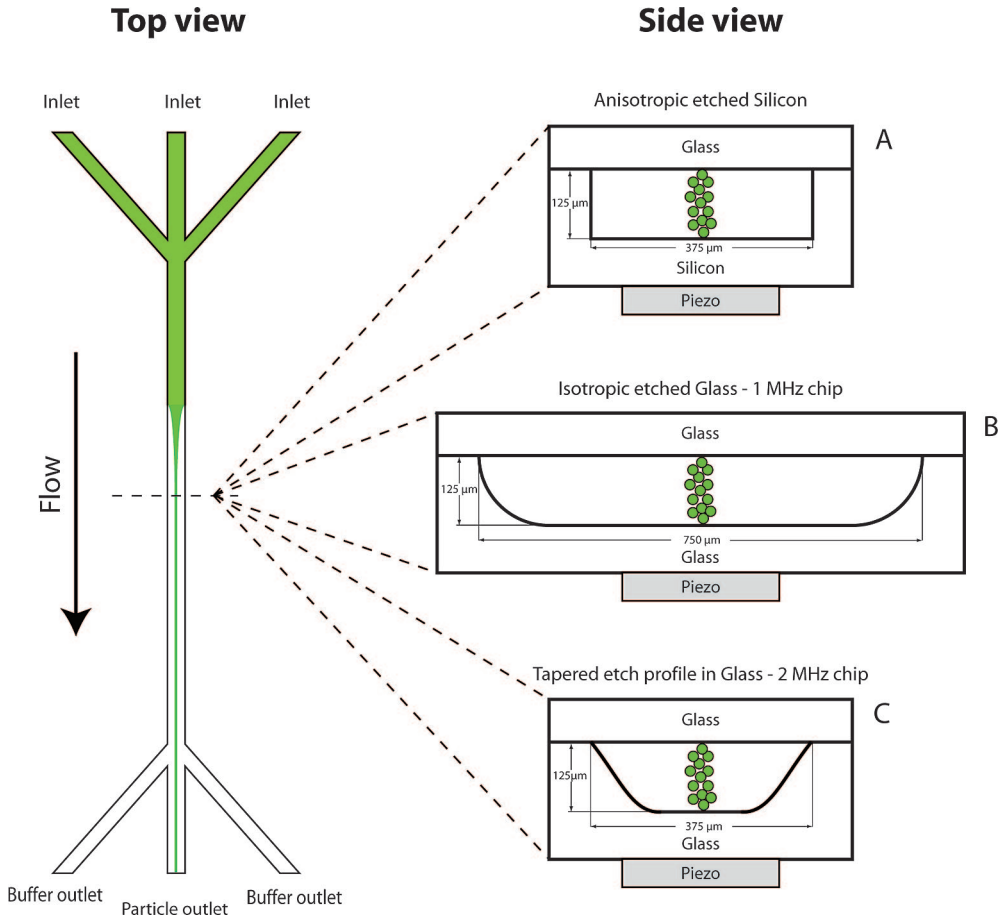

Figure 2. Schematic of the channel design and cross section of the different separation chips investigated. Panel A is the anisotropic silicon chip, panel B the isotropic 1 MHz glass chip, and panel C is the actual shape of the cross section of the 2 MHz glass chip.

between the side walls, or as a combination of both to create a two-dimensional force field.[22,34]

The way of actuation depends both on the chip design and in which direction the force field should be active. The most straightforward approach is to position the ultrasonic transducer with its direction of transmission parallel to the desired force field direction, Figure 1A. It is, however, also possible to create a lateral resonance perpendicular to the direction of transmission,[35] by positioning the transducer as seen in Figure 1B. This can be done with a standard transducer, a shear transducer, or using wedges to increase the amount of shear waves induced,[36] see Figure 1C.

Most devices using lateral resonances are fabricated in silicon using either anisotropic wet etching or deep reactive ion etching (DRIE). As silicon is a relatively expensive material and the fabrication process requires mask aligners for precise pattern transfer, alternative materials with easier fabrication processes are of interest. An alternative way of fabrication is by creating a sandwich structure with different layers defining the dimensions of the channel as well as the chip.[34] The precision in such a method is, however, limited and may cause problems when small tolerances are requested.

Polymers and glass are becoming preferred material bases in chemical and biomedical microdevices as they offer cheaper and less complex fabrication means. Designing polymer-based microdevices for ultrasonic actuation is, however, a nontrivial task due to the large acoustic attenuation. In this perspective, glass has several attractive properties beyond low cost such as optical

(34) Haake, A.; Neild, A.; Kim, D. H.; Ihm, J. E.; Sun, Y.; Dual, J.; Ju, B. K. *Ultrasound Med. Biol.* **2005**, *31*, 857–864.
(35) Nilsson, A.; Petersson, F.; Jonsson, H.; Laurell, T. *Lab Chip* **2004**, *4*, 131–135.
(36) Wiklund, M.; Gunther, C.; Lemor, R.; Jager, M.; Fuhr, G.; Hertz, H. M. *Lab Chip* **2006**, *6*, 1537–1544.

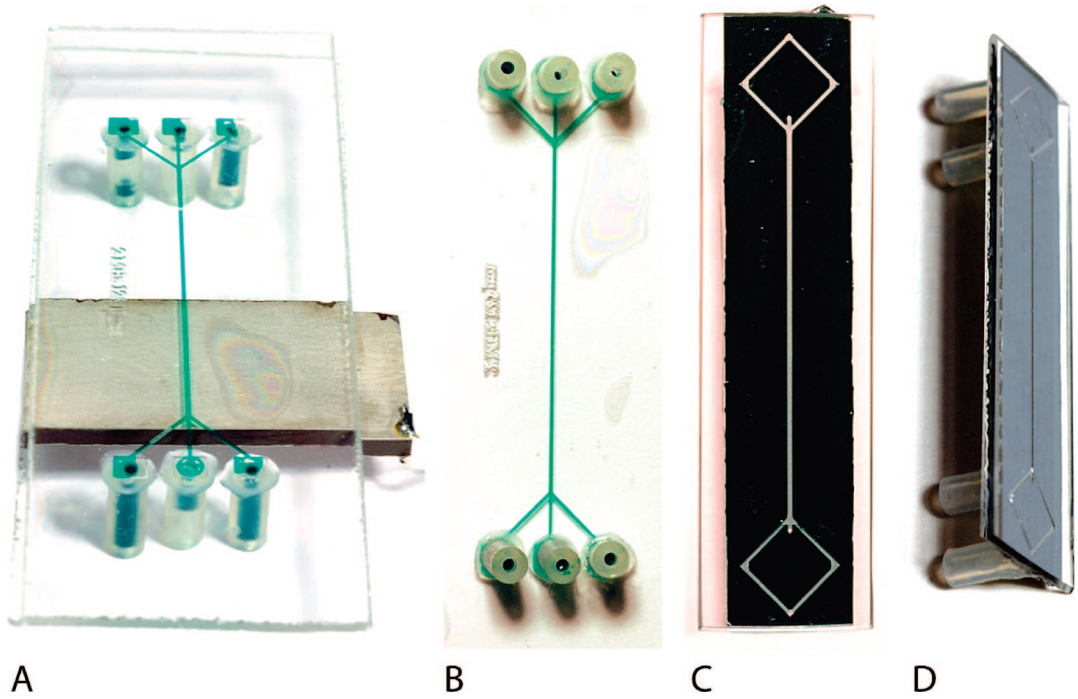

Figure 3. (A) Wet-etched glass chip with the piezoelectric element attached using ultrasonic gel. The back side of the glass chip with silicone tubing (B). The anisotropic silicon chip used for comparison can be seen in (C) and uses the same kind of silicone tubing for fluidic access from the back side (D).

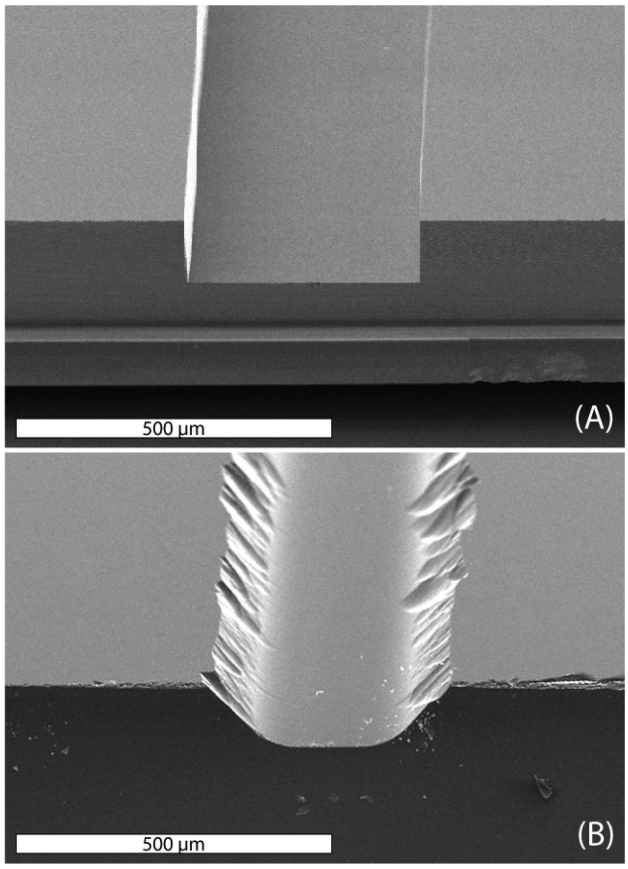

Figure 4. Scanning electron microscopy (SEM) images showing the cross section of the silicon (A) and glass (B) channel.

transparency, hydrophilic surface properties, electrical insulation, and good chemical resistance. Glass also bonds well to silicon and has a very low acoustic attenuation while being amenable to a multitude of micromachining processes. Isotropic wet etching is the most widely used fabrication method offering high performance at low cost. For more complex structures, DRIE[37] and molding/hot embossing[38] are also possible, but both techniques are more laborious and require advanced process equipment. Powder blasting can be employed to manufacture simple structures such as through holes and channels with limited demands in surface smoothness.[39]

The use of glass as the bulk material enables the use of microscopy techniques that have not been possible to use in previously reported acoustic silicon devices. One example is phase contrast imaging, a method commonly used to image cells or other small, transparent objects. Another example is Raman spectroscopy, where recent development projects cancer cell detection in clinical samples.[40] Raman spectroscopy can be anticipated to be combined with acoustic microchip cell handling for label-free on-chip cell sorting. The possibilities in achieving optimal light conditions are also vastly increased when a completely transparent material is used and both reflective and transmission microscopy can be used.

The technique of manipulating cells and particles in the microfluidic domain with acoustic forces relies on an acoustic standing wave generated in an enclosed fluid volume on a chip. The magnitude of the radiation force acting on the particles is strongly dependent on the radius of the particle (to the third

(37) Park, J. H.; Lee, N. E.; Lee, J.; Park, J. S.; Park, H. D. *Microelectron. Eng.* **2005**, *82*, 119–128.
(38) Takahashi, M.; Murakoshi, Y.; Maeda, R.; Hasegawa, K. *Microsyst. Technol.* **2007**, *13*, 379–384.
(39) Pu, Q. S.; Luttge, R.; Gardeniers, H.; van den Berg, A. *Electrophoresis* **2003**, *24*, 162–171.
(40) Chan, J. W.; Taylor, D. S.; Lane, S. M.; Zwerdling, T.; Tuscano, J.; Huser, T. *Anal. Chem.* **2008**, *6*, 2180–2187.

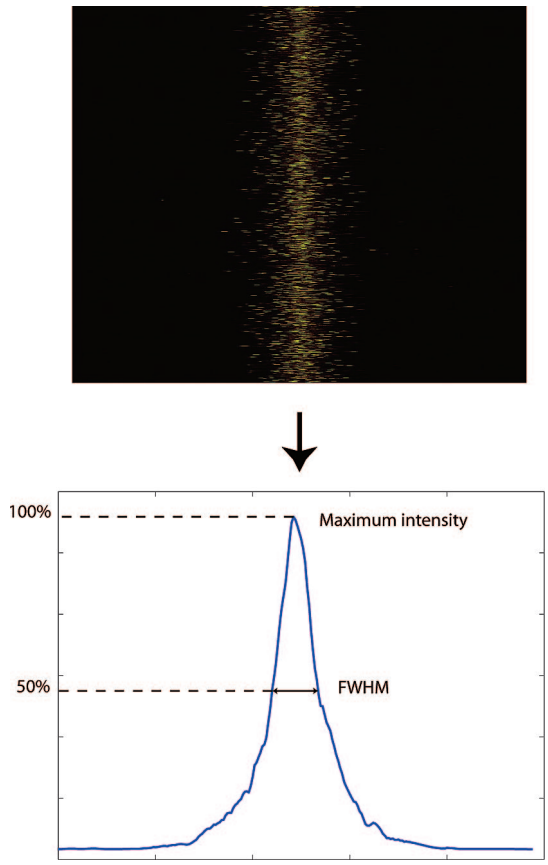

Figure 5. Line scans in the fluorescent image, top image, are averaged to achieve an intensity plot of the lateral particle distribution, lower image. For each confocal depth, the corresponding average full width at half-maximum value (fwhm) is calculated. The fwhm value is used as a representative width of the particle band, intensity-coded using the maximum intensity.

power) and proportional to the acoustic frequency.[41,42] The relationship between the density and compressibility of the particle and the surrounding medium will determine if the particle will move toward a pressure node or an antinode in the standing wave. For instance, a particle suspension flowing through a microchannel with a width of a half-wavelength will experience a radiation force concentrating all particles into a focused band in the center of the channel, see Figure 2. The laminar flow in the microchannel prevents the particles from dispersing again, and if the microchannel ends in a three-way split, the concentrated particles can be collected via the central outlet while the clear medium exits through the side outlets, and a simple separation/concentration step has been achieved.

Our most recent experimental data demonstrate that it is possible to design isotropically wet-etched glass devices that have particle manipulation properties comparable to what previously only has been reported for silicon-based substrates. This paper presents for the first time piezoelectrically actuated particle separation in isotropically etched all-glass microfluidic chips with separation properties matching the performance of silicon-based acoustic separators. The performance of the glass chip is compared to the corresponding anisotropically wet-etched silicon chip in a continuous flow separation application. A continuous medium exchange with live cells using acoustic forces in a glass chip is also presented.

MATERIALS AND METHODS

Design and Fabrication. A basic chip design with three inlets, three outlets, and a separation channel was used to compare the performance between the anisotropic silicon chip and the isotropic glass chip, see Figure 3. The separation performance was measured by focusing and separating 5 μm polyamide microparticles from their suspending medium. The particle suspension was a commercially available blood phantom (Danish Phantom Design, Jyllinge, Denmark) designed to mimic the viscosity, density, and sound velocity of human blood.

The glass and silicon chips were both designed to have a lateral resonance at 2 MHz. In order to achieve a single node at 2 MHz, the channel widths were designed to be 375 μm, i.e., $\lambda/2$ at 2 MHz in water. As the glass chips have an isotropic cross section, the widest part of the channel was designed to be 375 μm. Both chips were etched to a depth of 125 μm and had a 30 mm long separation channel. The glass chip was provided with separate connections, Figure 3B, to the side inlets and outlets, whereas the corresponding inlets and outlets in the silicon chip were united to one single outlet, Figure 3D.

The silicon separator was fabricated by means of double-sided photolithography and anisotropic wet etching using KOH. The chip was sealed by anodic bonding of a glass lid. A more detailed description of the microfabrication of the silicon chip can be found in Nilsson et al.[35] The cross section of the anisotropic separation channel was rectangular with vertical walls, see Figure 4A.

The glass chip was fabricated by wet etching 0.7 mm thick borosilicate chromium blanks (Telic Company, Valencia, CA), precoated with 0.5 μm positive resist, using a $HF/HNO_3/H_2O$ mixture. After etching, fluidic access holes were drilled using a 1 mm diamond glass drill. The etched and drilled chip was then cleaned in KOH in an ultrasonic bath and was thermally bonded to a clean borosilicate glass lid to form a sealed chip. Silicone tubing was glued to the fluidic access holes to hold standard $^1/_{16}$ in. Teflon tubing.

When etching glass in hydrofluoric acid, the resulting shape of the side walls depends on different parameters.[43–45] The adhesion between the masking layer and the glass, the pH or temperature in the etch solution, and the amount and type of stirring used are examples of parameters that can change the shape of the side walls.

The etched 2 MHz glass channel did not have the typical isotropic side-wall geometry, see Figure 4B. This is most likely caused by limited convective exchange of etch components in the zones underetching the mask. A similar channel with a twice as wide mask, with all other parameters unchanged, resulted in a perfect semicircular side wall.

Instrumentation. The chips were actuated using an 11 mm $\times$ 32 mm external PZT piezoelectric transducer (PZ26, Ferroperm Piezoceramics, Kvistgard, Denmark) with a thickness of 1 mm, corresponding to a fundamental resonance of 2 MHz. The

(41) Gorkov, L. P. *Sov. Phys. Dokl.* **1962**, *6*, 773–775.
(42) Laurell, T.; Petersson, F.; Nilsson, A. *Chem. Soc. Rev.* **2007**, *36*, 492–506.
(43) Kal, S.; Haldar, S.; Lahiri, S. K. *Microelectron. Reliab.* **1990**, *30*, 719–722.
(44) Parisi, G. I.; Haszko, S. E.; Rozgonyi, G. A. *J. Electrochem. Soc.* **1977**, *124*, 917–921.
(45) Spierings, G. *J. Mater. Sci.* **1993**, *28*, 6261–6273.

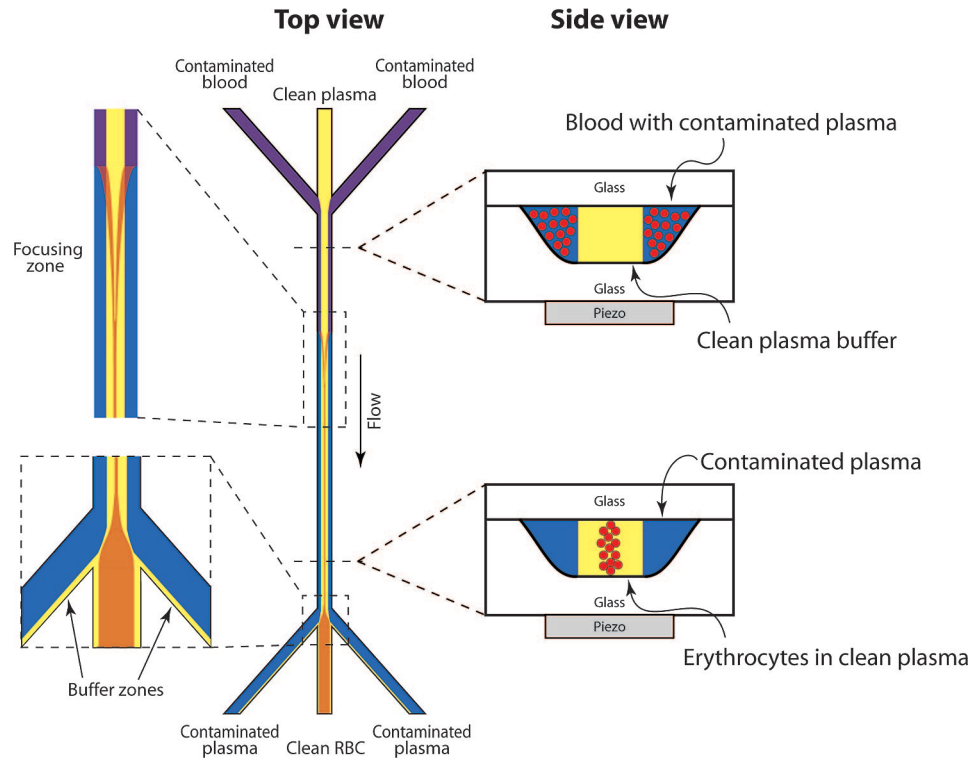

Figure 6. Blood wash and medium exchange principle. Contaminated blood enters from the side inlets, and clean plasma enters through the central inlet. The blood cells are switched over to the clean plasma by the acoustic radiation force and exit through the center outlet while the contaminated medium exits through the side outlets.

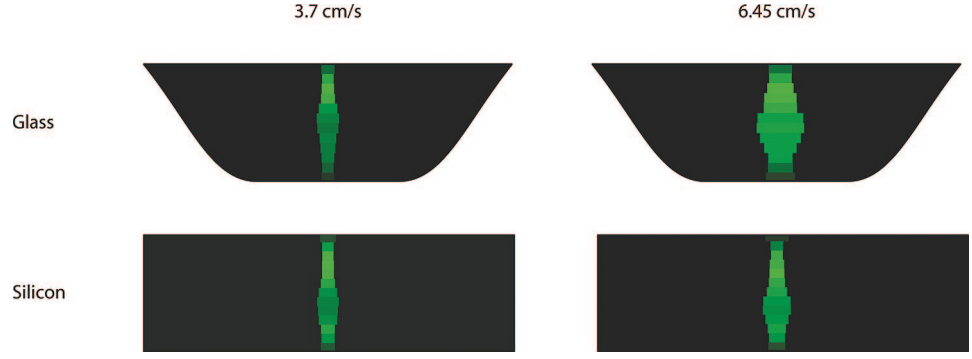

Figure 7. Cross-sectional view of the band formation in the channels based on confocal image data. The width of the particle band is decided by the fwhm value, and the intensity is correlated to the maximum intensity from the averages line scan. The widening of the particle band in the center of the channel is caused by the parabolic flow profile causing the particle in the center to have less time to focus into a narrow band.

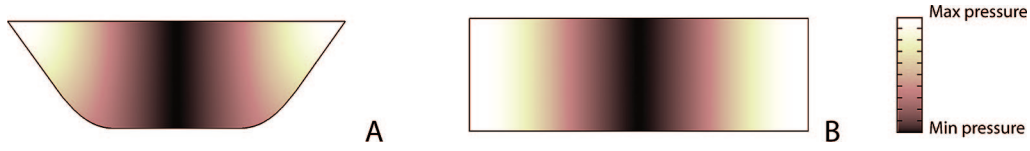

Figure 8. Squared pressure field, proportional to the acoustic force, in the glass cavity (A) and the silicon cavity (B) as simulated in COMSOL Multiphysics using eigen-frequency analysis. The simulation predicts the fundamental frequency to occur at 2.36 MHz for the glass chip and 2.0 MHz for the silicon chip.

transducer was applied to the back side of the chips using ultrasonic gel for good acoustic coupling and clamped in place, see Figure 3A. The transducer was actuated using a Hewlett-Packard 3325B waveform generator and an Amplifier Research 75A250 amplifier. The input power to the transducer was set at 0.5 W for all experiments and monitored using a Bird model 5000-EX digital power meter.

The confocal image data was acquired with an Olympus BX51WI microscope using the Fluoview 300 software. Fluorescent particles with a diameter of 4.1 μm were focused using the acoustic standing waves, and images of the focused particle band were taken at different depth in the channel using a motorized microscope stage and a step size of 10 μm. For each confocal image, the line scans were averaged to obtain the intensity profile

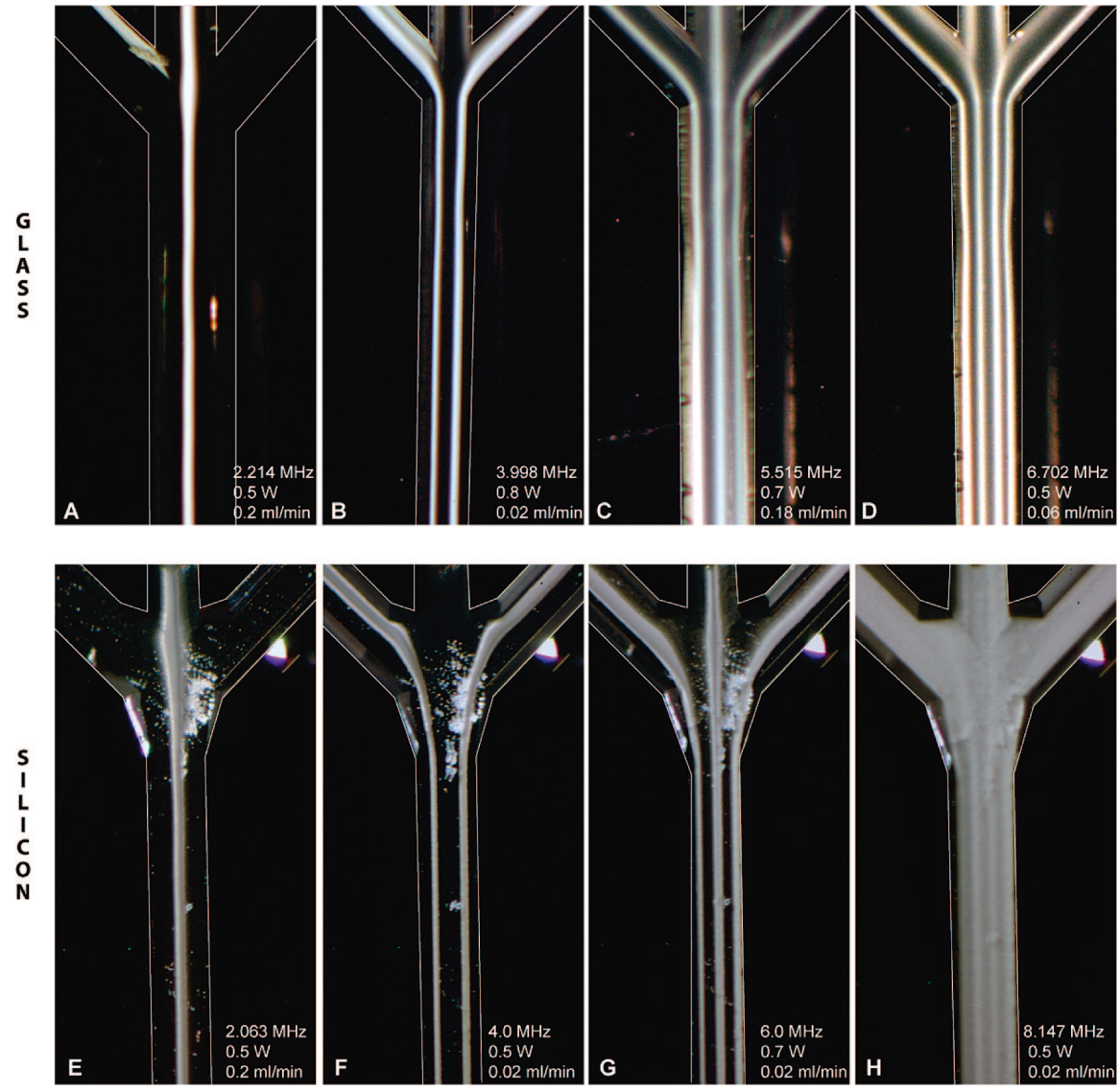

Figure 9. Particle focusing at higher harmonics: the glass chip at the top (A−D) and the silicon chip at the bottom (E−H). The channel walls have been outlined to improve the visibility.

of the lateral particle distribution and the full width at half-maximum (fwhm) and maximum intensity were calculated, see Figure 5. With the use of these data, a corresponding image was created in Adobe Illustrator where the fwhm value was used for the width of the particle band and color intensity of the band was correlated to the maximum intensity value for each confocal depth.

The separation efficiency was measured using a Beckman Coulter Multisizer 3 where the amount of particles in the center outlet was compared to the total amount of particles in all outlets. The samples were collected using 50 μL loops attached to an automated switch valve (Valco Instrument Company Inc.) while running the continuous separation.

Blood Washing and Medium Exchange. A continuous medium exchange with human blood was performed as an alternative mode of performance evaluation.[19] Evans blue (Merck AG, Darmstadt, Germany) was used to simulate a contaminant and was added to human whole blood. The erythrocytes were diluted to a hematocrit of 2% using pure plasma, and 180 μg/mL of Evans blue was added. The contaminated blood was infused through the side inlets at 70 μL/min while clean plasma was infused through the center inlet at 130 μL/min. The acoustic forces moved the erythrocytes from the contaminated plasma into the clean plasma fraction at the center of the channel, Figure 6. An input power of 0.8 W (8 Vpp) was used to ensure a good focusing of cells in the channel center. The erythrocytes transferred to the clean plasma were collected via the center outlet at 70 μL/min while the contaminated plasma continued to the side outlets and was withdrawn with 65 μL/min in each outlet. The different infusion/withdrawal rates ensured that a minor part of the clean buffer zone was directed to the side outlets and reduced the risk of contaminants spilling into the clean center outlet.

The blood washing efficiency was evaluated using a Labsystems Multiskan Multisoft photometric plate reader at an absorption wavelength of 595 nm. The ratio of absorbance in the contaminated media and the washed blood was compared, and an average of six different samples was calculated.

RESULTS AND DISCUSSION

Resonance Mode Characterization. By visual inspection, the best particle focusing for the chips occurred at 2.063 MHz for

the silicon chip and at 2.214 MHz for the glass chip. The particles were focused into the center of the channel with what appeared to be a uniform distribution of particles along the depth of the channel, much like the schematic image shown in Figure 2. To verify the particle distribution, a confocal microscopy scan was performed on fluorescent particles focused at two different flow velocities for each device. The result, seen in Figure 7, shows a slight bulging of the particle band in the center of the channel for both chips. This is most likely explained by the parabolic flow profile, giving a maximal flow velocity in the center of the channel causing particles there to be exposed to and focused by the acoustic standing wave for a shorter time period. The color intensity in the figure is a measure of the particle density, thus being higher in the tightly focused areas as compared to the widened zones.

With the use of COMSOL Multiphysics, an eigen-frequency analysis of the two chips was performed. The simulations predicted a fundamental frequency of 2.36 MHz for the glass chip and 2.0 MHz for the silicon chip. The squared pressure amplitudes, proportional to the acoustic radiation force, show a single pressure node in the center of both channels, see Figure 8. The simulations predicted the harmonics to appear at 4, 6, and 8 MHz for the silicon chip, whereas the glass chip showed a different behavior with harmonics at 4.3, 5.7, and 7.4 MHz.

The glass and silicon chip showed similar behavior in focusing particles when operated at their fundamental frequency, see Figure 9, parts A and E. The particle suspension used was well-focused and exited through the center outlet as expected. The first harmonic, twice the fundamental frequency, was tested to focus the particles into two bands, Figure 9, parts B and F. The glass chip displayed a slightly lower focusing efficiency, with broader particle bands, at this frequency, but the difference between the two materials was marginal.

At the second harmonic a more distinct difference between the chips was seen. The glass chip deviated from the expected frequency of 6.6 MHz and displayed a resonance at 5.515 MHz instead which correlates well with the resonance frequency predicted by the simulations. The focusing was, however, superior to that of the silicon chip where the flow rate had to be lowered to 0.02 mL/min at 0.5 W acoustic input power in order to get a reasonable picture of the band formation, which should be compared to 0.18 mL/min for the glass chip, Figure 9, parts C and G.

The same trend was repeated at the third harmonic where it hardly was possible to achieve a four-band focusing for the silicon chip, whereas the glass chip clearly showed a better focusing, Figure 9, parts D and H. The resonance frequency for the glass chip again differed from the expected 8.8 MHz and was now found at 6.702 MHz.

The reason for the deviation in resonance frequency is not clear but is most likely associated with the tapered shape of the side walls. For a rectangular geometry there is an analytical solution to the different lateral resonances. An isotropic channel is, however, more complex, and the resonances can only be determined by simulations.[46] As a comparison, a wet-etched glass chip with a fundamental resonance at 1.0 MHz, thus with twice the width of the 2 MHz chip, was tested. This chip showed a very nice isotropic cross section as opposed to the 2 MHz chip, see Figure 2B. The 1 MHz chip performed a single-band focusing at 1 MHz and was as expected slightly inferior to the 2 MHz chip in focusing strength due to the lower frequency. However, all of the harmonics for this chip were at the expected multiples of the fundamental frequency: 2.0, 3.0, and 4.0 MHz, respectively. Clearly, more work needs to be done in this area to fully understand how the geometry of the cross section of the chip affects the resonance frequencies.

(46) Townsend, R. J.; Hill, M.; Harris, N. R.; White, N. M. *Ultrasonics* **2006**, *44*, E467−E471.

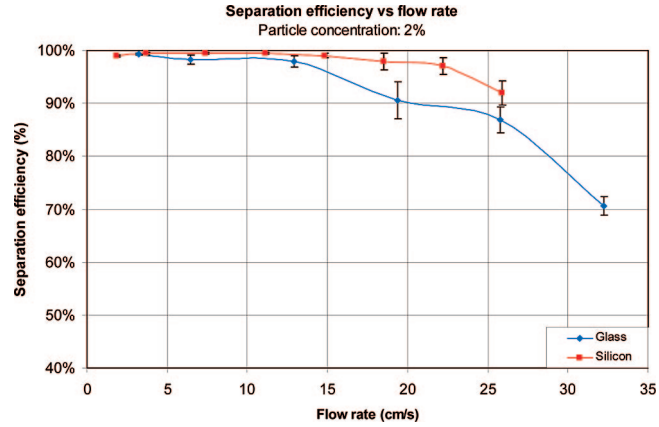

Figure 10. Separation efficiency vs the flow velocity at a particle concentration of 2% and an acoustic power input of 0.5 W. The performance of the two chips is similar although the silicon chip has slightly higher separation efficiency at higher flow velocities. The flow velocities used correspond to volumetric flow rates of 50−700 μL/min.

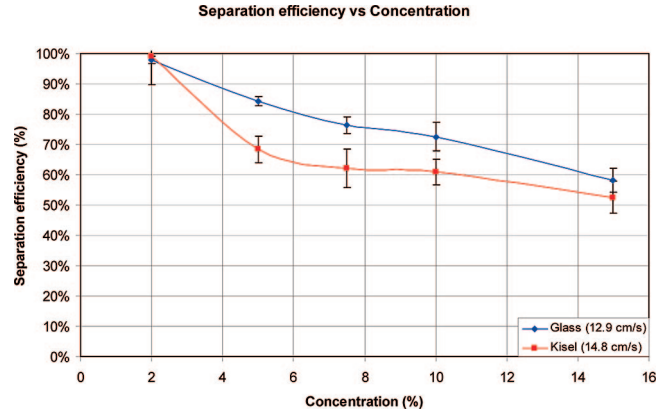

Figure 11. Separation efficiency plotted vs particle concentration. The two chips show a similar behavior although the silicon chip shows slightly lower separation efficiency at a slightly higher flow velocity.

Table 1. Comparison in Contaminant Removal Efficiency between a Glass Chip and a Silicon Chip[a]

	glass	silicon
separation efficiency (%)	92.8 ± 3.9	89.3 ± 5.8
contaminant removal (%)	97.1 ± 1.1	92.3 ± 1.2

[a] An amount of 180 μg/mL of Evan's blue was used as a contaminant, and the blood was diluted with plasma to a hematocrit of 2%.

Particle Focusing Efficiency. The separation efficiency of the particle separation in both glass and silicon chips versus an

increasing flow velocity can be seen in Figure 10. The separation efficiency clearly decreased as the flow velocity increased since the particles spent shorter time in the acoustic force field. At flow velocities up to 10 cm/s, the separation efficiency of the glass and silicon chip was comparable; however, at higher flow velocities the performance of the glass chip decreased as compared to the silicon chip.

While performing the experiments, volumetric flow rates were set on the syringe pumps. Due to the different cross sections of the chips, the flow velocities, and thus the retention times, of the particles will be different in the channels. The corresponding flow velocities were therefore calculated using a three-dimensional COMSOL simulation. For a volumetric flow of 100 μL/min, the glass chip has an average flow velocity of 6.45 cm/s, whereas the silicon chip, with a larger cross section, has an average flow velocity of 3.7 cm/s. Thus, for a given volumetric flow rate, the silicon chip will have a slower velocity and particles will spend more time in the force field.

The volumetric flow rate is many times a crucial factor, and commonly in microfluidic applications a volumetric flow of a few hundred microliters per minute is more than sufficient. If even higher flow rates are needed, several parallel channels actuated by a single transducer can be used.[17] It is also possible to increase the input power and create a stronger force field that will work even for higher flow rates. A higher input power may, however, result in an elevated temperature in the channel due to thermal losses in the transducer. This effect can be counteracted by using heat sinks or Peltier elements and work as a method of controlling the thermal environment on-chip.[26,28]

The separation efficiency for the silicon and glass chip with regards to the inlet sample concentration was compared, see Figure 11. As expected from earlier tests with silicon separation chips,[35] the separation efficiency decreases with particle concentrations ranging from 2−15%. The silicon and the glass chip show almost the same behavior for increasing concentration.

Medium Exchange in Cell Washing. Acoustic manipulation of cells offers a mode of noninvasive and noncontact spatial localization of cells in microfluidic systems. Most importantly, it has been shown in several experiments that acoustic cell manipulation does not induce any traceable adverse reactions to the exposure to an acoustic force field.[17,26,31] This fact opens up for the use of acoustic force manipulation to perform a set of unit operations that can be combined to design relevant bioanalytical sequences, integrated in a single microfluidic device. One such application is the possibility to perform a buffer exchange without having to expose the cells to a mechanically stressing event such as centrifugation. In this case a separation channel operated at its fundamental resonance and supplied with two buffer inlets as outlined in Figure 6 can switch cells from one buffer medium to another by the acoustophoretic process investigated herein.

During the medium exchange, a separation efficiency of 92.8% ± 3.9% was achieved and 97.1% ± 1.1% of the contaminant was removed from the blood using the glass chip, at a blood sample input flow rate of 70 μL/min. This can be compared to a separation efficiency of 89.3% ± 5.8% and a contaminant removal of 92.3% ± 1.2% for the silicon chip, see Table 1. If higher levels of medium exchange are requested it is advised that this process is repeated in a sequential step.

CONCLUSIONS

This paper reports for the first time an all-glass microfabricated chip for acoustic force control of cells and particles in a continuous microfluidic process. Essentially equal performance of the glass chip and its silicon counterpart is reported. The possibility to use acoustic forces in wet-etched glass channels may make microchip-based acoustic cell and particle manipulation widely available to the bioanalytical microfluidics community. The microfabrication of glass is less complicated than the silicon fabrication and also requires fewer and less expensive instruments. Glass is also a cheaper material, and the isotropic nature of the fabrication process allows for a larger degree of freedom in chip design.

The separation efficiency of the glass chips was above 97% for a 2% suspension for flow rates up to 200 μL/min. There are several ways of increasing the throughput in a glass chip while maintaining the high separation efficiency. A rather straightforward approach would be to use several parallel channels, but it is also possible to increase the input power. By increasing the input power the risk of elevating the temperature on-chip is increased, and measures to keep the temperature stable may have to be taken.

The acoustic glass separator has proven to be capable of handling the same tasks as the acoustic silicon separator, including particle separation and continuous medium exchange in human whole blood.

ACKNOWLEDGMENT

The authors thank the Swedish Research Council, the Carl Trygger Foundation, the Swedish Foundation for Strategic Research, the Crafoord Foundation, and the Royal Physiographic Society in Lund for financial support.

SUPPORTING INFORMATION AVAILABLE

A video showing the focusing of a particle suspension in a 2 MHz glass chip. This material is available free of charge via the Internet at http://pubs.acs.org.

Received for review March 19, 2008. Accepted April 14, 2008.

AC800572N